

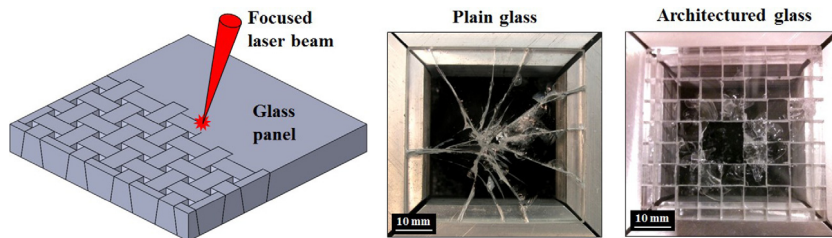
Carving 3D architectures within glass: Exploring new strategies to transform the mechanics and performance of materials



M. Mirkhalaf, J. Tanguay, F. Barthelat*

Department of Mechanical Engineering, McGill University, 817 Sherbrooke Street West, Montreal, Quebec, Canada H3A 2K6

GRAPHICAL ABSTRACT



ARTICLE INFO

Article history:

Received 26 November 2015

Received in revised form 9 February 2016

Available online 20 February 2016

Keywords:

Architected materials

Glass

Three-dimensional laser engraving

Topologically interlocked materials

Toughening mechanisms

Impact

Nonlinear deformations

ABSTRACT

Combining high strength, hardness and high toughness remains a tremendous challenge in materials engineering. Interestingly nature overcomes this limitation, with materials such as bone which display unusual combinations of these properties in spite of their weak constituents. In these materials, highly mineralized “building-blocks” provide stiffness and strength, while weak interfaces between the blocks channel non-linear deformation and trigger powerful toughening mechanisms. This strategy is also exploited in multilayered ceramics, fiber-reinforced composites, and more recently in topologically-interlocked materials. In this work we apply these concepts to the toughening of glass panels by incorporating internal architectures carved within the material using three-dimensional laser engraving. Glass is relatively stiff and hard but it has no microstructure, no inelastic deformation mechanism, low toughness and poor resistance to impacts. We demonstrate how introducing controlled architectures in glass completely changes how this material deforms and fails. In particular, our new architected glass panels can resist about two to four times more impact energy than plain glass. Our architected glass also displays non-linear deformation, progressive damage and failure contained within a few building blocks. This work demonstrates how micro-architecture, bio-inspiration and top-down fabrication strategies provide new pathways to transform the mechanics and performance of materials and structures.

© 2016 Elsevier Ltd. All rights reserved.

* Corresponding author.

E-mail address: francois.barthelat@mcgill.ca (F. Barthelat).

<http://dx.doi.org/10.1016/j.eml.2016.02.016>

2352–4316/© 2016 Elsevier Ltd. All rights reserved.

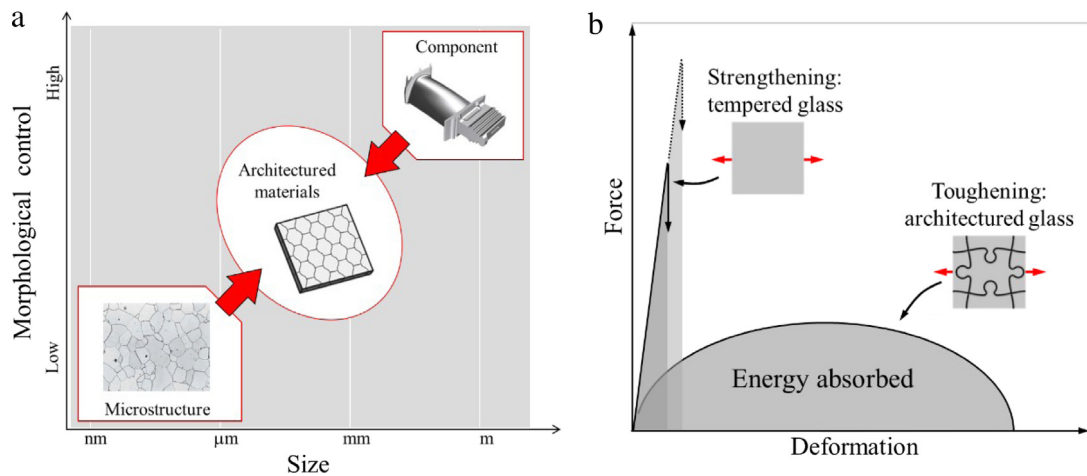


Fig. 1. General concept for dense architected materials: (a) an “Architecture” is created within the material, and at lengths scales intermediate between the component size and the microstructure (adapted from [9,15]). (b) While methods such as tempering aim at increasing strength, introducing an architecture aims at increasing toughness and energy absorption, by for example enabling large deformations at weak interfaces.

1. Introduction

Despite large efforts in material development and mechanics, some combinations of mechanical properties remain inaccessible to engineering materials [1,2]. For example materials which are simultaneously hard and tough are highly desirable for many applications, yet these properties remain mutually exclusive in engineering materials [1,3]. Interestingly, nature has overcome these limitations by incorporating intricate microstructures which are associated with powerful deformation and fracture mechanisms. For example, natural nacre [4,5], conch shell [6], tooth enamel [7], or bone [8] display unusual and attractive combinations of stiffness, hardness and toughness. The construction of these materials follows a “Universal” strategy where highly mineralized building blocks provide stiffness and hardness (platelets in nacre, mineralized fibrils and osteons in bone), and much weaker interfaces provide non-linear deformations, crack deflection and other powerful toughening mechanisms [9]. The idea of introducing weak interfaces to increase the mechanical performance of materials is counterintuitive, yet it is a common strategy in nature [9–12]. This strategy is also used in engineering materials such as multilayered ceramics and fiber reinforced composites, to generate crack deflection and controlled fiber pullout [13,14]. More recently, materials with more sophisticated three-dimensional architectures have emerged [15,16]. These materials introduce specific structural features at a length scale which is intermediate between the microstructure and the size of the component (Fig. 1(a)). Because the length scale associated with this architecture is larger than traditional microstructures, higher level of morphological control can be achieved with existing fabrication technologies, which is a requirement for a tight control of the deformation and fracture mechanisms. In dense architected materials, stiff building blocks are assembled in larger structures, and the interfaces between the blocks are weak so they can generate a wealth of non-linear deformation mechanisms and

crack deflection, which echo the concepts found in natural materials (Fig. 1(b)). In topologically interlocked materials (TIMs) the blocks have specific shapes which interlock to form architected materials with combined strength and toughness under transverse static [17,18] or impact loading [19]. These materials also display quasi-ductile behavior [20], localized damage [18], and re-manufacturability [21]. Different shapes of building blocks such as regular tetrahedral [19], osteomorphic [18], regular cubes [22,23], and buckyballs [20] have been used so far for TIMs. Building blocks have been made of materials such as polyvinyl chloride (PVC) [17,22], polyester [18], alloys of magnesium, titanium and aluminum [17,22], steel [17], ABS P400 polymer [16,21], alumina [23] or ice [24]. The blocks are fabricated first, and then assembled to fabricate materials and structures from the bottom-up.

In this work we present a new fabrication technique based on a top-down strategy, where weak interfaces are carved within a hard but brittle material. We use glass as a base material, and three-dimensional laser engraving to generate weak interfaces within the bulk of the material [25,26]. Glass is not only an ideal model material to explore the laser engraving approach, it is also a material which is used for its optical properties, hardness, durability, thermal and chemical stability in countless applications. Glass has however relatively poor fracture toughness and impact resistance, which restricts its potentially broader range of applications. Glass can be strengthened by tempering, which consists of generating residual compressive stress state within a thin layer of material at the surface, by either heat treatment or ion implantation. Once a crack is initiated, tempered glass has however no resistance to crack propagation, which results in catastrophic fracture and complete destruction of the component. Laminating glass is another strategy which consists of intercalating glass layers with softer polymeric layers to keep glass fragments together in case of fracture. Tempering and laminating can be used simultaneously, but none of these methods truly increases the fracture toughness of glass (Fig. 1(b)). The idea of introducing an

“architecture” within glass to improve its deformation mechanisms and toughness therefore offers interesting perspectives from a fundamental point of view as well as for practical applications.

2. Architected glass panels: design and fabrication

In this work we explored the mechanics and performance of architected glass panels composed of topologically interlocked blocks. The three-dimensional geometry of the individual blocks was obtained by truncating a disphenoid tetrahedron (whose faces are four identical isosceles triangles, Fig. 2(a)). The lower face of the block corresponds to the medial cross-section of the tetrahedron, a square surface of dimensions $l \times l$. The upper surface corresponds to a rectangular cross section located at a distance h from the medial section. Two of the sides are tilted inward and the other two outward by the same angle θ , the interlocking angle [27]. The geometry of the individual blocks was therefore fully defined by the size of their base l , height h and the interlocking angle θ (Fig. 2(b)). The architected panel is composed of a square array of these blocks, rotated and arranged in order to form a dense, interlocked structure. Once in place in the panel, each individual block (shown in gray in Fig. 2(c)) is constrained along the in-plane x and y directions because it is in direct contact with the adjacent blocks (shown in blue in Fig. 2(c)). Translations along the out-of-plane z direction are also constrained, because of the combination of friction and interlocking angle θ . Likewise, the rotations of individual blocks about axes x , y and z are constrained. This pattern can be repeated in both x and y directions to form large panels, which are held in place and stabilized by a stiff frame [16,19]. In this work we studied the behavior of panels made of 7×7 blocks (Fig. 2(d)). With this structure in place, the displacement of each block from the effect of external loads must be accommodated by frictional sliding between the blocks as well as deformation of the individual blocks. Using this strategy, the deformation mechanism of a panel made of stiff but brittle blocks is augmented with sliding at the interfaces between the blocks, following the concept shown in Fig. 1(b). Previously described TIMs were based on full regular tetrahedra (i.e. whose faces are equilateral triangles [19,20]), which resulted in non-planar surfaces for the panel, reduced contact areas between the blocks and also imposed a fixed angle of $\theta = 35.2^\circ$ for the interlocking angle arising from the geometry of the regular tetrahedron. In this work we use truncated tetrahedra to achieve planar surfaces on the panels and to maximize contact surface area. In addition we used non-regular tetrahedra so that the interlocking angle θ could be varied.

In previous work on topologically interlocked materials, the blocks were first fabricated individually and then assembled from the bottom-up [18,19]. Here we used a different fabrication strategy which can be characterized as “top-down”. The base material was a borosilicate optical grade 263 M glass panel with the lateral dimensions $L \times L$ of 50.8 by 50.8 mm and thickness of 3.175 mm. The three dimensional contours of interlocked blocks in a panel were then created numerically using Matlab (R2014a, MA, USA), and with the dimensions $l = 6.375$ mm and

$h = 3.175$ mm. Different interlocking angles ranging from $\theta = 0^\circ$ to $\theta = 20^\circ$ were explored. The three dimensional model was then physically engraved within the borosilicate glass panels using a three-dimensional laser engraver (Model Vitrolux, Vitro Laser Solutions UG, Minden, Germany) equipped with a pulsed UV laser (355 nm, 0.5 W cw pumped, 4 kHz repetition rate, 4–5 ns pulse duration). The laser engraver focused a nano-second ultraviolet laser beam into the glass, generating micro-defects at the successive focal points (Fig. 3(a)). Optical imaging of the microdefects show that they are elongated along the direction of the laser beam (z axis in Fig. 3(a)), possibly due to spherical aberration in the focusing lens. Arrays of these defects generated weak interfaces which can guide the deformation and failure behavior of the resulting materials [25,26]. The engraved panels were attached to a tape and were loaded in bending at different locations to completely separate each block following the engraved interfaces. This process involved mixed mode fracture for interlocking angles larger than 0, but models by Cotterell and Rice [28] and recent fracture experiments on engraved glass [25] show that there is little difference in apparent toughness when the angle of the engraved interfaced is increased from 0° to 10° . The samples were then transferred into an adjustable aluminum frame equipped with power screws which were used to control the in-plane pre-compression on the samples. Once the panel was secured in the frame, the tape was peeled off and the assembly was ready for testing (Fig. 3(b)). In some cases we glued the blocks with an ionomer (Surlyn 9320, Dupont, ON, CA). Ionomers are polymers which rely on electrostatic cross-links which can break and reform upon deformation, much like hydrogen bonds in natural materials. This molecular feature imparts ionomers with simultaneous high deformation and high strength, making these polymers suitable to increase toughness [29,30].

Fig. 3(c) shows a representative scanning electron micrograph of an engraved interfaces after fracture. The surface is irregular and shows characteristics of glass fracture with multiple mirror sites (Fig. 3(c)), indicating multiple crack initiation points [31]. Between these sites, the surface shows multiple ripples, possibly Wallner lines resulting from shifts of local stress due to the interaction between the engraved micro-defects. Laser profilometry (using Wyko NT3300 interferometer, MA, US) on the fractured surfaces reveals a morphology which may be decomposed into a surface waviness (amplitude $\sim 3\text{--}5 \mu\text{m}$, wavelength $\sim 100 \mu\text{m}$) and a surface roughness (amplitude $\sim 0.3\text{--}0.5 \mu\text{m}$, wavelength $\sim 10 \mu\text{m}$). Fig. 3(d) and (e) show the waviness and roughness of the fracture surfaces, as functions of the angle of the engraved interfaces (i.e. interlocking angle θ). Both waviness and roughness are minimal for $\theta = 0^\circ$. In this configuration the longest dimension of the engraved microdefects are contained within the engraved planes, which as a result produce the “cleanest” cuts and the smoother surfaces. Propagating cracks along interfaces at $\theta = 1.5^\circ$ and higher probably formed steps between the defects, producing rougher surfaces.

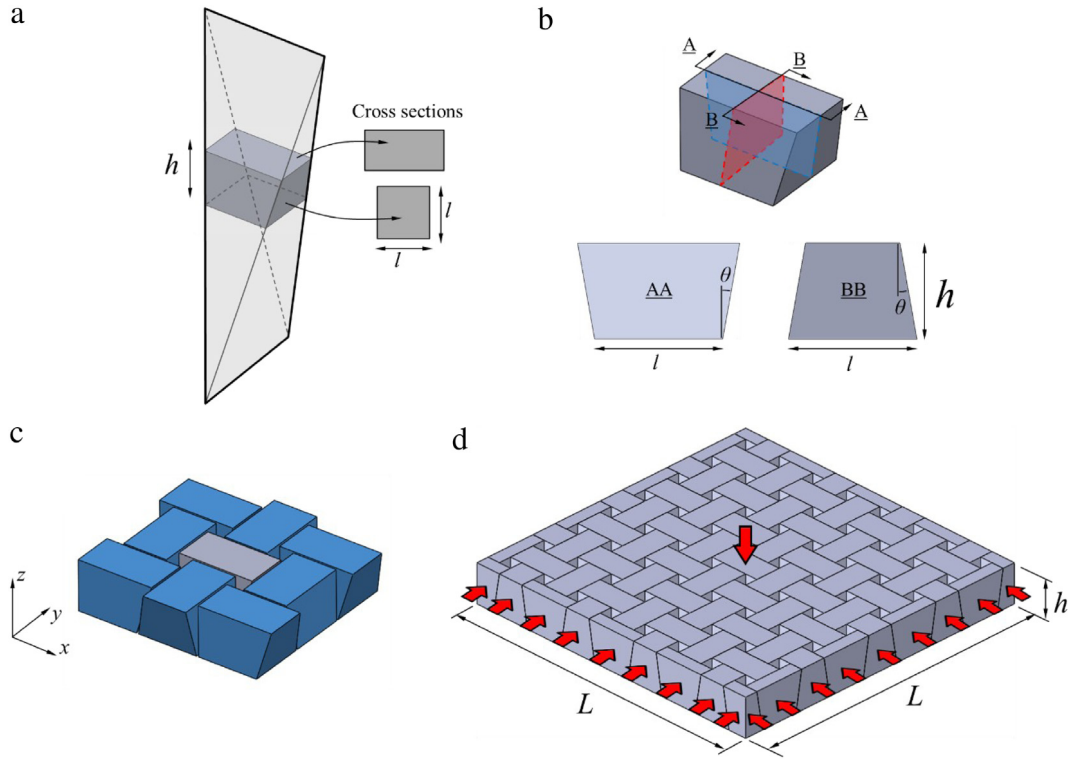


Fig. 2. Overview of the architected glass panel. (a) The geometry of the individual building blocks is obtained from truncating a tetrahedron. (b) Geometry of the building blocks, showing the interlocking angle θ . (c) Once assembled, the translation and rotation of individual blocks (in gray) in any direction is confined by the neighboring blocks (in blue) so that the panel is “topologically interlocked”. (d) The 7×7 simply supported architected panel used in this study. For testing the panel is placed in a frame that generates the confinement required for interlocking, and a transverse force is applied at the center of the panel. (For interpretation of the references to color in this figure legend, the reader is referred to the web version of this article.)

3. Quasi-static mechanical performance

In this work we focused on the performance of the panel when subjected to a transverse force or a transverse impact, which are both loading configurations representative of many applications such as architectural glass in buildings, vehicle windows, safety glasses, transparent armors, protective eyewear or transparent structures. We applied the transverse load in the center of the panel, keeping the upper and lower surfaces traction-free while the edges of the panels were resting on a supporting frame. The assembly was then placed in a universal testing machine (5 kN MTS Dual column loading stage, MN., USA) mounted with a 25 mm diameter steel ball for loading. During the test, the ball was driven into the center of the panel at a constant displacement rate of $20 \mu\text{m/s}$, while force and displacement were recorded (Fig. 4(a)). We tested plain borosilicate glass panels as reference, as well as a series of engraved borosilicate glass panels with different interlocking angles. For each configuration, three samples were prepared and tested. Fig. 4(c) shows typical force–displacement curves, showing major differences in terms of performance and failure mode between plain and engraved panels. Plain glass panels failed at a force of almost 2 kN, in a brittle fashion and at a deflection smaller than 0.5 mm. Failure was sudden and catastrophic, with multiple cracks emanating from the indentation site and extending to the edges

of the panel (Fig. 4(b)). The nature of the failure mode indicates a flexural failure, which is representative of the type of failure for larger glass panels [31] (failure due to contact stresses from a spherical indenter would have produced conical cracks). All the architected glass panels tested here showed a much lower strength (10–15 times lower), but a much larger deflection (5–6 times higher) compared to plain glass. We also observed a different deformation mode, where during the test the blocks were progressively pushed out of the panel. Failure occurred by complete push out of the indented blocks, which occurred at a deflection of about 3 mm (which matches the thickness of the panel $t = 3.175 \text{ mm}$). Failure was confined to only a few blocks, the rest of the panel remaining intact (Fig. 4(b)). Fig. 4(d) shows the force–deflection for the engraved panels only. All architected panels produced bell-shaped curves, with different responses for different interlocking angles.

Fig. 5 shows the stiffness, strength and energy absorption (area under the force–displacement curve) as functions of the interlocking angle. Interestingly the engraved panel can withstand a significant amount of force even for $\theta = 0^\circ$, probably because of the interlocking generated by the waviness of the engraved interfaces. All properties increased for higher interlocking angles up to $\theta = 2.5^\circ$, because of stronger interlocking from the angle and also possibly from the slight increase of surface roughness (Fig. 3(d), (e)). Beyond $\theta = 2.5^\circ$ the stiffness kept increasing as the interlocking increased, but we also observed that

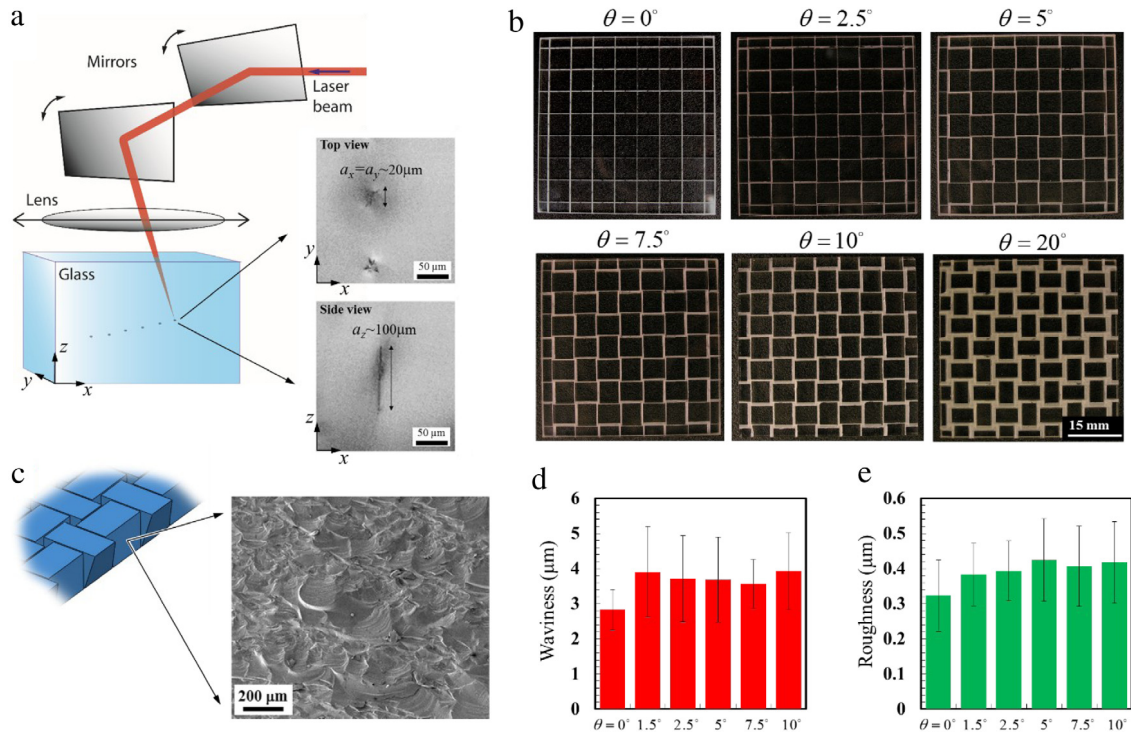


Fig. 3. Fabrication and morphology of architected glass panels. (a) A nanosecond pulsed laser focused beam creates micro-defects at its focal point. The micro-defects are elongated along the z-direction. Arrays of these defects define the weak interfaces between individual blocks. (b) Architected glass panel with different interlocking angles. (c) SEM image of an engraved interface after fracture; (d) waviness and (e) roughness from laser profilometry and as function of interlocking angle.

the blocks did not slide as much as for small interlocking angles. Instead, damage and fracture of individual blocks were observed at the early stages of loading. This change of deformation and failure mode resulted in a slightly decreasing strength and energy absorption (Fig. 5(b), (c)). The increase of stiffness, slightly different failure mode and decrease of strength and energy absorption beyond $\theta = 1.5^\circ$ must be attributed to change in interlocking angles only, since the roughness remained almost constant for that range of angles (Fig. 3(d), (e)).

These results suggest several concurrent deformation modes for the engraved panels. First, the deflection of the panel may be generated by tilting of the blocks, a mechanism which can be captured by trust line analysis [19], a well established method for analysis of the deformation of the arches and domes [32]. The second deformation mode, which from our observations was prominent here, is the sliding of the blocks on one another. The jamming of the blocks upon deflection generates in plane compression which results in frictional forces, which can be amplified by increasing the interlocking angle. Finally, a third deformation mode corresponds to the partial damage of the blocks near the interfaces, which we observed for large interlocking angles. Among the architected panels tested here, the best performance in terms of combined strength and energy absorption was obtained with an interlocking angle of $\theta = 2.5^\circ$. This result depends on the base material, size and possibly number of the blocks, and additional experiments and modeling are needed to optimize this system. As expected,

the stiffness and strength of the architected glass panel are lower than plain glass since weak interfaces were introduced in the system. The maximum displacement is however much greater, 3 mm for the architected glass compared to about 0.45 mm for plain glass. The area under the force–deflection curve provides a measure of the “energy to fracture” for the glass panel. This energy was about 300 mJ for the architected glass with $\theta = 2.5^\circ$, which is 10% lower than plain glass (330 mJ). By this measure the architected glass is therefore slightly inferior to plain glass. In the case of plain glass panels however, a large portion of the energy to fracture is stored in the form of elastic strain energy, which upon fracture is suddenly released. This sudden burst of energy is not absorbed by the material and can propagate to other parts of the structure, possibly creating additional damage over large volumes. In general, a brittle material like glass can only absorb a small fraction of the area under the force–deflection curve, by the creation of new cracks. This phenomenon is well-documented for the fracture testing of brittle materials [33] or for brittle ceramics pulverizing upon impact, for which despite extensive cracking, the fracture energy (i.e. creation of new surfaces) typically forms only 1%–2% of the impact energy [34]. In the plain glass panel tested here we counted about 25 cracks emanating from the impact point (Fig. 4(b)), resulting in a total surface area for the cracked material of approximately $2 \times 10^{-3} \text{ m}^2$. Using a critical energy release rate of $G_c = 3 \text{ J/m}^2$ for glass [35], we then determined the energy consumed by the plain glass panel

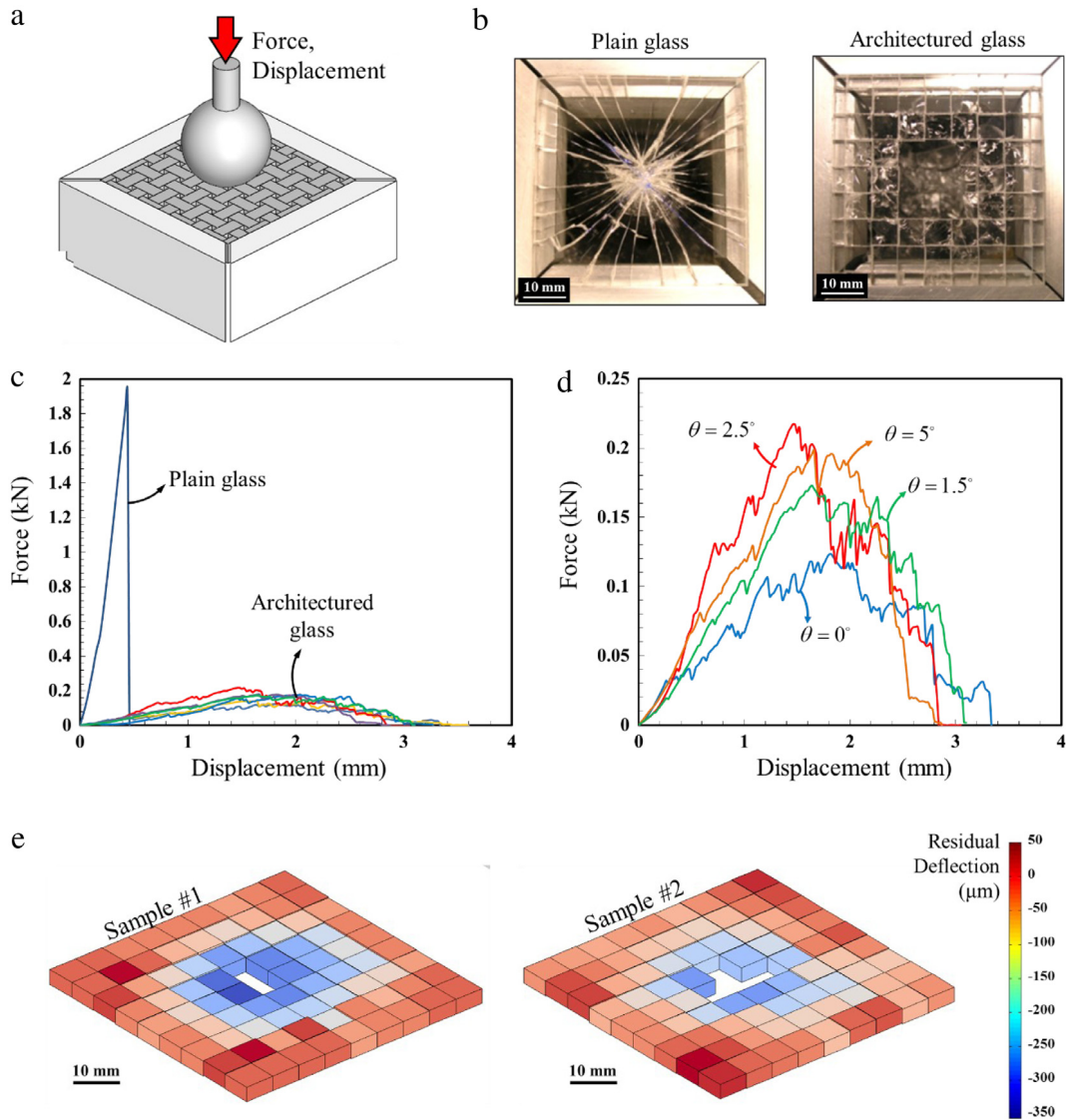


Fig. 4. (a) Quasi-static test setup. (b) Typical post mortem samples for plain and architected glass panels. (c) Force–displacement curves for plain and architected glass panels. (d) Force–displacement curves for the architected glass panels only, showing the effect of interlocking angle on the mechanical response. (e) Deflection of individual blocks measured at the onset of softening on two different samples.

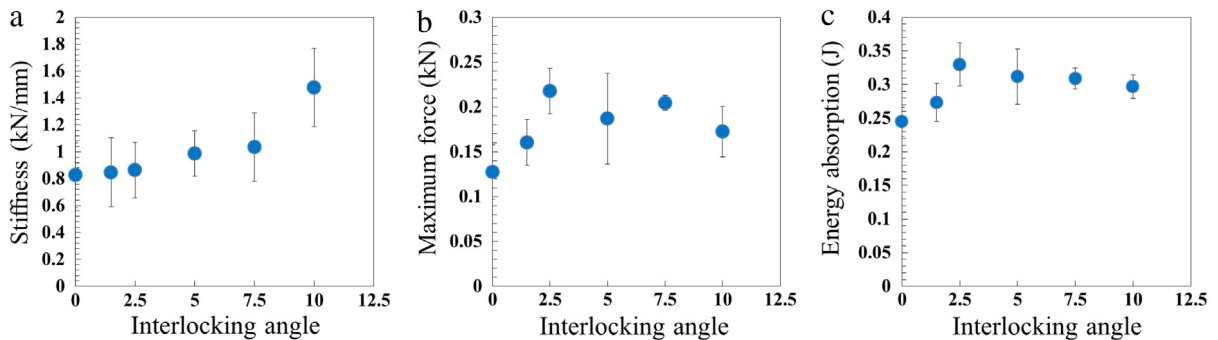


Fig. 5. Mechanical properties of the architected glass panels plotted as a function of interlocking angle: (a) stiffness, (b) strength and (c) energy absorption.

by the formation of new cracks at 6 mJ. Only 1.8% of the energy to fracture was therefore actually absorbed by the plain glass panel (which is consistent with previous work on brittle materials [33,34]). For the architected panels, the failure mode and energy absorption mechanisms were completely different. The energy to fracture obtained from the area under the force–deflection curve truly represents the energy dissipated in the material, because the panel fails progressively and “gracefully”, with little dynamic effects. For the architected panels this energy is dissipated by friction between the blocks. By this measure, which better represents the impact resistance of the material, the best engraved glass panel we tested in this work ($\theta = 2.5^\circ$) absorbed about 50 times more energy than the plain glass panel. In terms of management of mechanical energy upon failure, the architected glass therefore largely out-performs plain glass.

We finally determined the displacement of individual blocks in the panel. The architected panel in its holding frame was placed on a precision bench where the vertical (out-of-plane) position of each individual block was measured with a micrometer dial indicator. The sample was then tested in puncture, but the test was interrupted at the onset of damage, i.e. when 1–2 blocks were pushed out of the panel (which corresponded to the onset of softening on the force–displacement curve). The sample was then returned to the precision bench, where the vertical position of the blocks was measured again. The difference of position before and after the puncture test gave the residual displacement of each block. The results (Fig. 4(e)) show residual deflection in the range of 300–400 μm over a “zone of influence” of only about 1–2 blocks around the damage site. This residual displacement highlights the amount and extent of the frictional sliding at the interfaces, the dissipative mechanism which is responsible for energy absorption in the architected panel.

4. Impact performance

Materials and structure usually display failure modes and mechanical performances which are functions of loading rate [36]. Here we assessed the performance of the panels at high deformation rates by impacting them with a 67.3 g steel ball, which had the same diameter as the ball used for the quasi-static tests (25 mm, Fig. 6(a)). The glass panels were placed in the same holder and frame used for the quasi-static tests, and the assembly was positioned so the ball impacted the panel in its center. The ball was released from a controlled height using an electromagnet mounted on a vertical column. The ball was then accelerated by gravity, and we measured its velocity just prior to impact using an infrared velocimeter (Smart Timer LE 21B, Science first, FL, USA).

The protocol to assess the impact resistance was as follows: the steel ball was first released from a small height (300 mm) onto the panel. If the panel survived this first strike, the height was increased by 5 mm, and the impact test was repeated. This procedure was repeated until the sample failed, i.e. when visible cracks propagated within the plain glass samples or when at least one block

was pushed-out of the architected glass panel (since these two materials displayed different failure modes, different criteria for what is considered failure also had to be used). Typical impact velocities at failures were $V_0 = 3$ to 6.5 m/s. For each configuration, three samples were tested. The kinetic energy of the ball just prior to impact was calculated using $K = \frac{1}{2} mV_0^2$, and the kinetic energy required to fail the panel was then taken as a measure of impact resistance. This testing protocol involved multiple impacts of increasing energy until the panel failed. In this procedure damage may progressively accumulate in the panel, which may ultimately decrease its final impact resistance. To test this hypothesis we performed impact tests on five architected panels (with $\theta = 2.5^\circ$), but using an impact energy equal to the impact resistance of the same material measured after multiple impacts. Out of five panels, two failed upon the first impact, and three failed upon the second one. We repeated these additional impact tests on plain glass panels, with similar results. These results indicated that the final impact resistance of the plain and architected glass panels did not significantly change when they were impacted multiple times prior to final failure. Fig. 6(b) shows that the failure modes from impact are identical to those observed for the quasi-static tests: multiple flexural cracks in the plain glass panel, and push out of blocks in the architected glass panel. Fig. 6(c) summarizes the results of the impact tests. The energy required to break the plain glass panels was 330 ± 30 mJ ($N = 3$), which is identical to the energy required to fracture plain glass in quasi-static conditions (area under the force–deflection curve). The energy required to fail the architected glass was significantly higher than for plain glass, most likely because of the frictional energy dissipation at the interface. This mechanism imparted additional resistance to impact even for the case $\theta = 0^\circ$, increasing up to 530 ± 25 mJ (60% higher than for plain glass) for $\theta = 2.5^\circ$. As for the quasi-static case, we found that the impact resistance did not improve further for interlocking angles larger than 2.5° , which we again attributed to excessive interlocking between the blocks. The enhanced energy dissipation capabilities of the architected panel can be further demonstrated by measuring the coefficient of restitution (COR) for the impact, which was obtained by dividing the velocity of the steel ball after rebound V_R by its velocity before impact V_0 . [37]. We measured the COR using impact energies of 40 and 175 mJ, which correspond to about 10% and 50% of the average energy required to fracture the plain glass panels. The results (Fig. 6(d)) show that at low impact energy, the COR for plain and architected glass panels is not significantly different, indicating that the mechanisms for energy storage and absorption are identical in both systems. A higher impact energy the COR decreases slightly for plain glass, by a small margin which is not significant. However, the COR becomes much smaller, decreasing by almost 50%. These results suggest that low impact energies are not sufficient to slide the blocks, but that beyond a threshold of impact energy the blocks start sliding on one another, adding a frictional dissipative mechanism to the system which translates into a lowered COR. We also measured the deflection of individual blocks upon

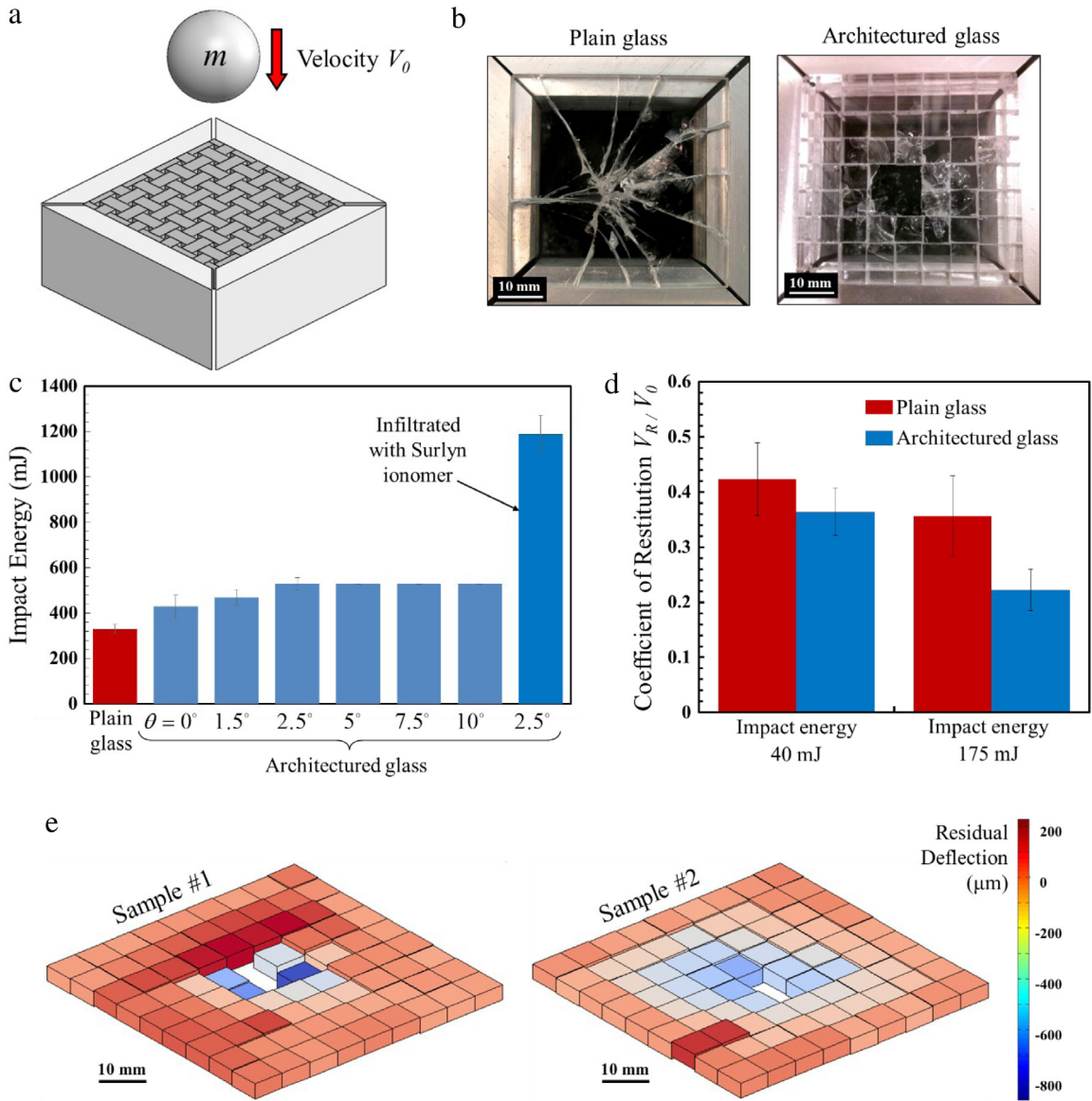


Fig. 6. (a) Ball impact setup. (b) Typical post mortem samples for plain and architected glass panels. (c) Impact energy required to break the panels. (d) Coefficient of restitution is a measure of the “rebound” of the steel ball from the panel. The architected glass panel absorbs more kinetic energy. (e) Deflection of individual blocks measured at the onset of damage on two different samples.

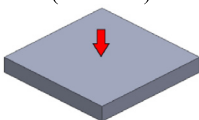
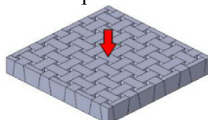
the onset of damage for the architected panel, using the same method as we used for the samples tested in quasi-static condition. The results shown on Fig. 6(e) for two different samples show residual deflections which are much higher than in the quasi-static case, reaching about 800 μm . The number of blocks with residual deflection is also larger, with a “zone of influence” which extends in the entire panel. Some blocks also appeared to have been pushed upwards during the impact. This result confirms that in impact situation the frictional sliding of the blocks is a prominent deformation and dissipative mechanism in the architected panel.

While the energy absorbed and stored in the plain glass panel was the same in quasi-static or impact loading, our result show very different results for the architected

panel at these two loading rates. In impact loading the architected plate could absorb up to 530 mJ, which is about 1.75 times higher than the energy absorbed by the same system in quasi-static conditions. Similar rate dependencies have been reported in the literature on the effect of rate on the energy absorption capabilities of composite materials [36,38]. For the architected glass panel, the most likely explanation for this large difference is the sliding of the blocks which appears to be more extensive in magnitude and spreading in the impact case (Figs. 4(e) and 6(e)). A possible explanation is the overloading of the system in the impact situation, and the additional resistance of the plate provided by the inertia of the individual blocks. Other possible mechanisms include rate effects in the frictional mechanisms between

Table 1

Summary of key properties for the architected glass panel. The quantitative properties are provided relative to the plain glass panel, which is used as reference.

	Plain glass panel (reference)	Architected glass panel
		
Relative surface hardness	1	1
Relative flexural stiffness	1	0.07
Relative flexural strength	1	0.07
Relative energy absorbed	1	50
Relative impact resistance	1	2 (4 with Surlyn)
Failure mode	Catastrophic	Graceful
Damage tolerance, multi-hit capabilities	None	Very high
Optical clarity	Excellent	Acceptable, depends on application

the blocks, and attenuation of the elastic waves by the periodic structure of the material [39].

Finally, we tested architected glass panels where the blocks were glued with the ionomer Surlyn. The results show that the plastic deformations of Surlyn greatly enhance the energy dissipation properties of the architected glass panels (Fig. 6(c)). The impact resistance of the Surlyn infiltrated architected glass was about four times higher than that of the plain glass, and ~ 2.5 times higher than that of the non-infiltrated architected glass.

5. Summary

Combining hardness, strength, toughness and impact resistance remains a tremendous challenge in engineering materials. Bioinspiration and architecture may provide new pathways to achieving these properties simultaneously. In particular, a promising strategy is to generate stiffness and strength with blocks of controlled geometry, while generating deformation and toughness with the weak interfaces between the blocks. Here we apply these concepts on glass panels, using a top-down fabrication approach where interfaces are carved within the material using three-dimensional laser engraving. Glass is an amorphous material with no microstructure and no toughening mechanisms, and as a result it has no inelastic deformation capabilities when subjected to tensile or flexural loads at ambient temperatures. This work demonstrates how the introduction of a controlled architecture at a length scale which is intermediate between the molecular scale and the scale of the component completely transforms the way glass deforms and fractures. The key properties for the architected glass panel, in comparison to the reference plain glass, are shown in Table 1. Plain glass panels can store a large amount of impact energy, in the form of elastic strain energy which can be restituted and provide “rebound” of the impact. However, if the strength of glass is reached, failure is catastrophic and propagates over large volumes, often destroying the entire component. In contrast, the deformation and failure of the architected glass

is dominated by the collective sliding and push-out of the individual blocks. In this process the panels dissipate impact energy by frictional sliding, or by viscoplastic deformation of an interface material. The failure is progressive, and damage is confined to a few blocks only, making it a better impact-resistant material compared to plain glass. The experiments presented here show that this process depends on the shape of the blocks (interlocking angle), the roughness of the engraved interface, the interface material and the rate of loading. Deformation and fracture of the architected panel may also depend on the geometry, size and arrangement of the blocks, and on the degree of confinement provided by the external frame. These mechanistic aspects will deserve further investigations using experiments and modeling tools to optimize overall mechanical performance. Engraving preserves the surface hardness, and the impact resistance is improved by a factor of almost 2. These improvements are achieved at the expense of stiffness and strength, but future optimization work may alleviate the effects of this trade-off. An important feature of the architecture introduced here is its very high morphological fidelity. For example, in the architected glass panels presented here the interlocking angle could be adjusted by increments of only 0.5° to adjust mechanical performance. In the future, this fabrication strategy can therefore be used to fine tune the architecture of material to obtain optimal performance. Finally, in the material fabricated in this work the optical clarity decreased due to the engraving. Further work is also needed in this respect in order to tune the engraving process to the requirement of specific applications in terms of optical clarity and mechanical performance.

Acknowledgments

This work was supported by an I2I grant from the Natural Sciences and Engineering Research Council of Canada and by the Fonds de Recherche du Québec—Nature et Technologies. The authors are grateful to Pascal Hubert for the MTS dual column loading stage, and to Richard Chromik and Lisa Lee for their help with the profilometer.

References

- [1] R.O. Ritchie, The conflicts between strength and toughness, *Nature Mater.* 10 (2011) 817–822.
- [2] U.G. Wegst, H. Bai, E. Saiz, A.P. Tomsia, R.O. Ritchie, Bioinspired structural materials, *Nat. Mater.* (2014).
- [3] A.R. Studart, Bioinspired ceramics: Turning brittleness into toughness, *Nat. Mater.* 13 (2014) 433–435.
- [4] A.P. Jackson, J.F.V. Vincent, R.M. Turner, The mechanical design of Nacre, *Proc. R. Soc. B* 234 (1988) 415–440.
- [5] F. Barthelat, H. Tang, P.D. Zavattieri, C.M. Li, H.D. Espinosa, On the mechanics of mother-of-pearl: a key feature in the material hierarchical structure, *J. Mech. Phys. Solids* 55 (2007) 306–337.
- [6] S. Kamat, X. Su, R. Ballarini, A. Heuer, Structural basis for the fracture toughness of the shell of the conch *Strombus gigas*, *Nature* 405 (2000) 1036–1040.
- [7] S. Habelitz, S. Marshall, G. Marshall, M. Balooch, Mechanical properties of human dental enamel on the nanometre scale, *Arch. Oral Biol.* 46 (2001) 173–183.
- [8] K.J. Koester, J.W. Ager III, R.O. Ritchie, The true toughness of human cortical bone measured with realistically short cracks, *Nature Mater.* 7 (2008) 672–677.
- [9] F. Barthelat, Architected materials in engineering and biology: fabrication, structure, mechanics and performance, *Int. Mater. Rev.* 60 (2015) 413–430.
- [10] P. Fratzl, I. Burgert, H.S. Gupta, On the role of interface polymers for the mechanics of natural polymeric composites, *Phys. Chem. Chem. Phys.* 6 (2004) 5575–5579.
- [11] J.W.C. Dunlop, R. Weinkamer, P. Fratzl, Artful interfaces within biological materials, *Mater. Today* 14 (2011) 70–78.
- [12] F. Barthelat, Z. Yin, M.J. Buehler, Structure and mechanics of interfaces in biological materials, *Nat. Rev. Mater.* (2016) in press.
- [13] W.J. Clegg, K. Kendall, N.M. Alford, T.W. Button, J.D. Birchall, A simple way to make tough ceramics, *Nature* 347 (1990) 455–457.
- [14] A.G. Evans, Perspective on the development of high-toughness ceramics, *J. Am. Ceram. Soc.* 73 (1990) 187–206.
- [15] Y. Brechet, J.D. Embury, Architected materials: Expanding materials space, *Scr. Mater.* 68 (2013) 1–3.
- [16] Y. Feng, T. Siegmund, E. Habtour, J. Riddick, Impact mechanics of topologically interlocked material assemblies, *Int. J. Impact Eng.* 75 (2015) 140–149.
- [17] S. Schaare, A. Dyskin, Y. Estrin, S. Arndt, E. Pasternak, A. Kanel-Belov, Point loading of assemblies of interlocked cube-shaped elements, *Internat. J. Engrg. Sci.* 46 (2008) 1228–1238.
- [18] A.V. Dyskin, Y. Estrin, E. Pasternak, H.C. Khor, A.J. Kanel-Belov, Fracture resistant structures based on topological interlocking with non-planar contacts, *Adv. Energy Mater.* 5 (2003) 116–119.
- [19] S. Khandelwal, T. Siegmund, R. Cipra, J. Bolton, Transverse loading of cellular topologically interlocked materials, *Internat. J. Solids Structures* 49 (2012) 2394–2403.
- [20] A. Dyskin, Y. Estrin, A. Kanel-Belov, E. Pasternak, Topological interlocking of platonic solids: a way to new materials and structures, *Phil. Mag. Lett.* 83 (2003) 197–203.
- [21] A. Mather, R. Cipra, T. Siegmund, Structural integrity during remanufacture of a topologically interlocked material, *Int. J. Struct. Integr.* 3 (2012) 61–78.
- [22] Y. Estrin, A. Dyskin, E. Pasternak, S. Schaare, S. Stanchits, A. Kanel-Belov, Negative stiffness of a layer with topologically interlocked elements, *Scr. Mater.* 50 (2004) 291–294.
- [23] M. Dugue, M. Fivel, Y. Brechet, R. Dendievel, Indentation of interlocked assemblies: 3D discrete simulations and experiments, *Comput. Mater. Sci.* 79 (2013) 591–598.
- [24] A. Autruffe, F. Pelloux, C. Brugger, P. Duval, Y. Bréchet, M. Fivel, Indentation behaviour of interlocked structures made of ice: influence of the friction coefficient, *Adv. Energy Mater.* 9 (2007) 664–666.
- [25] M. Mirkhalaf, A.K. Dastjerdi, F. Barthelat, Overcoming the brittleness of glass through bio-inspiration and micro-architecture, *Nat. Commun.* 5 (2014) 3166.
- [26] M. Mirkhalaf, F. Barthelat, A laser-engraved glass duplicating the structure, mechanics and performance of natural nacre, *Bioinspiration Biomimetics* 10 (2015) 026005.
- [27] M. Brocato, L. Mondardini, A new type of stone dome based on Abeille's bond, *Internat. J. Solids Structures* 49 (2012) 1786–1801.
- [28] B. Cotterell, J.R. Rice, Slightly curved or kinked cracks, *Int. J. Fract.* 16 (1980) 155–169.
- [29] H. Liu, F. Chen, B. Liu, G. Estep, J. Zhang, Super toughened poly (lactic acid) ternary blends by simultaneous dynamic vulcanization and interfacial compatibilization, *Macromolecules* 43 (2010) 6058–6066.
- [30] H. Keskkula, D. Paul, Toughening agents for engineering polymers, in: *Rubber Toughened Engineering Plastics*, Springer, 1994, pp. 136–164.
- [31] J.D. Quinn, *Fractography of Ceramics and Glasses*, National Institute of Standards and Technology, 2007.
- [32] P. Block, M. DeJong, J. Ochsendorf, As hangs the flexible line: Equilibrium of masonry arches, *Nexus Netw. J.* 8 (2006) 13–24.
- [33] S.M. Barinov, Work-of-fracture determination for brittle materials, *J. Mater. Sci. Lett.* 12 (1993) 674–676.
- [34] G.T. Camacho, M. Ortiz, Computational modelling of impact damage in brittle materials, *Internat. J. Solids Structures* 33 (1996) 2899–2938.
- [35] B. Lawn, *Fracture of Brittle Solids*, Cambridge university press, 1993.
- [36] S.M. Lee, P. Zahuta, Instrumented impact and static indentation of composites, *J. Compos. Mater.* 25 (1991) 204–222.
- [37] J. Calsamiglia, S.W. Kennedy, A. Chatterjee, A. Ruina, J.T. Jenkins, Anomalous frictional behavior in collisions of thin disks, *J. Appl. Mech.* 66 (1999) 146–152.
- [38] Z. Fan, J. Shen, G. Lu, D. Ruan, Energy absorption of sandwich tubes under lateral loading, in: *Dynamic Behavior of Materials*, Vol. 1, Springer, 2013, pp. 321–328.
- [39] B. Davies, A. King, P. Newman, A. Minett, C.R. Dunstan, H. Zreiqat, Hypothesis: Bones toughness arises from the suppression of elastic waves, *Sci. Rep.* 4 (2014).